Computer modelling of metal - oxide interfaces



1997 J. Phys.: Condens. Matter 9 5709

(http://iopscience.iop.org/0953-8984/9/27/004)

J. Phys.: Condens. Matter **9** (1997) 5709–5717. Printed in the UK PII: S0953-8984(97)80186-5

# Computer modelling of metal–oxide interfaces

J Purton†‡§‖, S C Parker‡¶ and D W Bullett†

† School of Physics, University of Bath, Claverton Down, Bath BA2 7AY, UK
‡ School of Chemistry, University of Bath, Claverton Down, Bath BA2 7AY, UK

Received 9 December 1996, in final form 26 March 1997

**Abstract.** We have used atomistic simulations to model oxide–metal interfaces. We have, for the first time, allowed the atoms on both sides of the interface to relax. The efficiency of the computational method means that calculations can be performed on complex interfaces containing several thousand atoms and do not require an arbitrary definition of the image plane to model the electrostatics across the dielectric discontinuity. We demonstrate the viability of the approach and the effect of relaxation on a range of MgO–Ag interfaces. Defective and faceted interfaces, as well as the ideal case, have been studied. The latter was chosen for comparison with previous theoretical calculations and experimental results. The wetting angle (133.6°) and work of adhesion (0.26 J $m^{-2}$) for MgO{100}–Ag{100} are in reasonable agreement with experiment. As with *ab initio* electronic structure calculations the silver atoms have been shown to favour the position above the oxygen site.

## 1. Introduction

Knowledge of metal–ceramic interfaces is central to understanding a wide range of materials of technological importance, e.g. heterogeneous catalysts, corrosion and device fabrication. The properties of these metal–ceramic composites depend critically on the interaction across the metal–ceramic interface. There have been several reviews concerning the relationship between the mechanical behaviour and the chemical bonding at metal–ceramic interfaces [1–3]. The driving force for the formation of a metal–ceramic interface is the decrease in free energy which is given by the Dupre equation [1, 4],

$$\Delta G = \sigma_c + \sigma_m - \sigma_{mc}$$

where $\sigma_m$ and $\sigma_c$ are the surface energies of the metal and ceramic respectively and $\sigma_{mc}$ is the metal–ceramic interfacial energy. In the absence of plastic deformation across the interface the free energy change is identical to the work of adhesion ($W_{ad}$), which is the energy required to separate a unit area of interface to the two component surfaces,

$$\sigma_{mc} = \sigma_m + \sigma_c - W_{ad}.$$

§ Present address: Department of Geology, Wills Memorial Building, University of Bristol, Queen's Road, Bristol BS8 1RJ, UK.
‖ E-mail address: j.a.purton@bris.ac.uk
¶ E-mail address: s.c.parker@bath.ac.uk

0953-8984/97/275709+09$19.50  

Thus as the work of adhesion increases (i.e. bonding across the interface improves) the interfacial energy decreases. Experimentally the work of adhesion can be derived from the wetting angle ($\phi$) using the Young–Dupre equation [1],

$$W_{ad} = \sigma_m(1 + \cos\phi).$$

The Young–Dupre equation indicates that if $\phi < 90^\circ$ wetting of the substrate occurs.

Previous theoretical studies concerning thin metal films on oxides may be divided into two groups. The first is based on electronic structure methods using either the local density [5–8] or periodic Hartree–Fock [9] approximation. These *ab initio* methods require large amounts of computer time and are restricted to the study of a few tens of atoms. To obtain a realistic description of metal–ceramic interfaces a large number of species need to be considered. This is addressed by the second group of theoretical studies based on atomistic simulations where a potential model is required that incorporates the main features of the bonding across the interface yet remains computationally efficient and as flexible as possible. One such model has been developed by Duffy and co-workers [10, 11]. In this model the interaction between the metal and ceramic is composed of short-range repulsive interactions an attractive electrostatic image interaction [12, 13]. The image interaction is modified by introducing a cut-off in the wave-vector of the induced charge distribution in the metal. The image interaction model has been applied to perfect surfaces of Ag–MgO and Au–MgO [10] and more recently to surfaces containing point defects [14]. This pioneering work has provided a valuable insight into the bonding at metal–oxide interfaces.

An alternative method for the calculation of the image interaction, the discrete classical model (DCM), has been developed by Finnis *et al* [15] and is not restricted to planar surfaces. We have introduced the DCM into our atomistic simulation codes to evaluate the electrostatic interaction across the interface and have applied this model to determine the structure and energetics of MgO–Ag interfaces. The reasons for studying this system are (i) the small mismatch in lattice parameter implies that the interface can be produced experimentally without introducing many defects, (ii) there is little chemical interaction across the surface, and (iii) comparison with previous electronic structure and atomistic calculations should provide a validation of the model. We have then extended the range of applications to consider defective and stepped surfaces.

## 2. Computational method

We have investigated the stability of interfaces between magnesium oxide and silver using lattice energy minimization techniques. The interface calculations were performed on slabs of material containing 31 layers of MgO and ten metal layers at either end. The simulation requires a reliable potential model for each of three components: (i) within the ceramic oxide, MgO; (ii) within the metal, Ag; and (iii) between the oxide and the metal.

(i) *Ceramic oxide MgO.* A rigid-ion model was assumed (i.e. no shells were included) and formal charges were assigned to the ions. For surfaces, which are periodic in two dimensions, the Madelung energy was evaluated using the method of Parry [16]. The two-body short-range potentials were of the form

$$E = A\exp(-r/\rho) - C/r^6$$

and were derived by empirically fitting to the bulk properties of MgO [17].

(ii) *Metal Ag.* In contrast, calculation of the surface properties of metals requires many-body potentials [18]. These were developed around the second-moment approximation to

the tight-binding model [19] and simplified by Sutton and Chen [20], who devised a many-body potential based around the Lennard-Jones potential. This potential has been shown to accurately determine the energy and relaxations of {100}, {110}, {111}, and reconstructed {110} surfaces [21, 22] of silver. The form of the potential is

$$E = \varepsilon\left[\frac{1}{2}\sum_{i\neq j}\sum V(r_{ij}) - c\sum_{i}\rho_i^{1/2}\right]$$

where

$$V(r) = (a/r)^n$$

and

$$\rho_i = \sum_{i\neq j}[a/r]^m.$$

(iii) *Metal–ceramic.* Stoneham and Tasker [12, 13] recognized the importance of the image interaction across the interface. The classical continuum model has been shown to break down within 3 Å of the surface [15]. To overcome these shortcomings Finnis *et al* [15, 23] developed the discrete classical model (DCM) by considering the interaction of a point charge with an aluminium surface. The DCM model generates point charges, $q(i)$, and dipole moments, $\rho_\gamma(i)$, on the metal atoms which have the same electrostatic potential at each site. The total induced charge on the metal is equal and opposite to the external charge $q^{ext}$,

$$\sum_i q(i) = -q^{ext}.$$

The electrostatic potential at site $i$ is given by

$$V = C(i,j)q_{(j)} + C_\gamma(i,j)\rho_\gamma(j) + V_{(i)}^{ext}$$

where $V^{ext}(i)$ is the potential due to the external charge. The matrices $C(i,j)$ and $C_\gamma(i,j)$ are due to the Coulomb potential and electric field respectively at site $i$ due to a charge at site $j$. These are periodically repeated in two dimensions and can easily be calculated within the Parry method. The diagonal elements of $C(i,j)$ include a potential, $U$, due to the metal atom itself. As in previous calculations [15] the value of $U$ was set equal to the self-energy of a sphere, with the radius of the Wigner–Seitz radius, of uniform charge. The charges and dipole moments on the metal atoms are calculated by solving a set of linear equations [15] and the electrostatic interaction between the oxide and metal due to the DCM is

$$E^{DCM} = \tfrac{1}{2}q(i)V^{ext}(i) - \tfrac{1}{2}\rho(i)E_\gamma^{ext}(i) + \tfrac{1}{2}V.$$

The dipole moments are given in terms of the polarizability, $\alpha$, of the metal atoms,

$$\rho_\gamma(i) = \alpha E_\gamma(i).$$

The polarization term was obtained, following Finnis *et al* [15], by assuming the polarizability, $\alpha$, of the metal atom is equal to $4/3\pi r^3$, where $r$ is the Wigner–Seitz radius of the metal.

The image interaction across the interface is balanced by short-range potentials between the oxygen and metal and the magnesium and metal. The potentials (table 1) were obtained by a least-squares fit to interaction energies obtained from electron-gas calculations [24, 25]. The dispersion term was obtained by using the polarizability, $\alpha$, of the metal atom in the Slater–Kirkwood [26, 27] expression to estimate the dispersion coefficient. This method was also used by Duffy *et al* [10] to evaluate the dispersion interaction.

**Table 1.** Short-range potential parameters for Silver–$X_{ion}$ were determined by a least-squares fit to energies obtained from electron-gas calculations. The form of the short-range potential is $E_{(Ag-X)} = A\exp^{(r_{(Ag-X)}/\rho_{(Ag-X)})} - C/r^6_{(Ag-X)}$.

| Interaction | $A$ (eV) | $\rho$ (Å) | $C$ (eV Å$^{-6}$) |
|---|---|---|---|
| Ag–O | 4970.5966 | 0.2493 | 95.00 |
| Ag–Mg | 982.7081 | 0.3364 | 0.00 |
| Ag–Li | 1115.0589 | 0.2875 | 0.00 |
| Ag–K | 3740.9570 | 0.2933 | 0.00 |
| Ag–Ca | 2889.8696 | 0.3042 | 0.00 |
| Ag–Sr | 3920.0000 | 0.3068 | 0.00 |
| Ag–Ba | 3861.6784 | 0.3201 | 0.00 |

## 3. Results

In this first study we investigated both the MgO{100}–Ag{100} and MgO{110}–Ag{110} interfaces to determine the relative importance of the electrostatic interaction and the magnitude of the relaxation of oxide and metal. In addition, we ascertained how these were modified by the possible reconstruction of the interface and the presence of point defects. However, we started with the ideal interfaces so as to compare our results with previous work on this interface.

### *3.1. Ideal interface*

Our simulations of the MgO{100}–Ag{100} interface considered the three possible configurations for the absorption site of Ag atoms: (i) directly above $Mg^{2+}$; (ii) above the $O^{2-}$ ion; and (iii) above the interstitial site (figure 1(a)). The minimum-energy configuration for the Ag atoms was found to be above the $O^{2-}$ ions (table 2). This is in agreement with the *ab initio* electronic structure calculations [5, 6, 9], but differs from the model of Duffy and co-workers [10, 11] (table 3). This difference is probably due to the sensitivity of the atomistic simulation models to the choice of short-range potential parameters rather than the treatment of the electrostatic component. The small energy differences are supported by the experimental results of Trampert *et al* [28] where both Ag above Mg and Ag above O are observed, although this has been refuted by Guénard *et al* [29], who found Ag atoms only above $O^{2-}$ ions. We calculate the optimum Ag–$O^{2-}$ distance to be 2.6 Å, which compares well with values obtained with *ab initio* calculations [5–9] and the experimental distance of 2.43 Å [29].

As discussed in section 1, the strength of the adhesion across the interface is measured in terms of the work of adhesion and the binding energy (table 2). Our calculated work of adhesion and wetting angle (0.26 J m$^{-2}$ and 1.33°) are in reasonable agreement with the experimentally determined values of 0.45 J m$^{-2}$ and $1.35 \pm 5°$ [28] respectively. The DCM contributes approximately 0.05 J m$^{-2}$ to the work of adhesion, most of which is due to polarization (less than 0.01 J m$^{-2}$ is from the monopole–monopole interaction). Table 3 lists the works of adhesion and wetting angles obtained from the other computational methods. The image model [10, 11] and the full-potential linearized muffin tin orbital (FLMTO) [5] method overestimate the work of adhesion in comparison to experiment. Much better agreement is found with the full-potential linearized augmented planewave (FLAPW) [6] and Hartree–Fock [9] calculations.

The most stable configuration for the MgO{110}–Ag{110} interface (figure 1(b)) was for

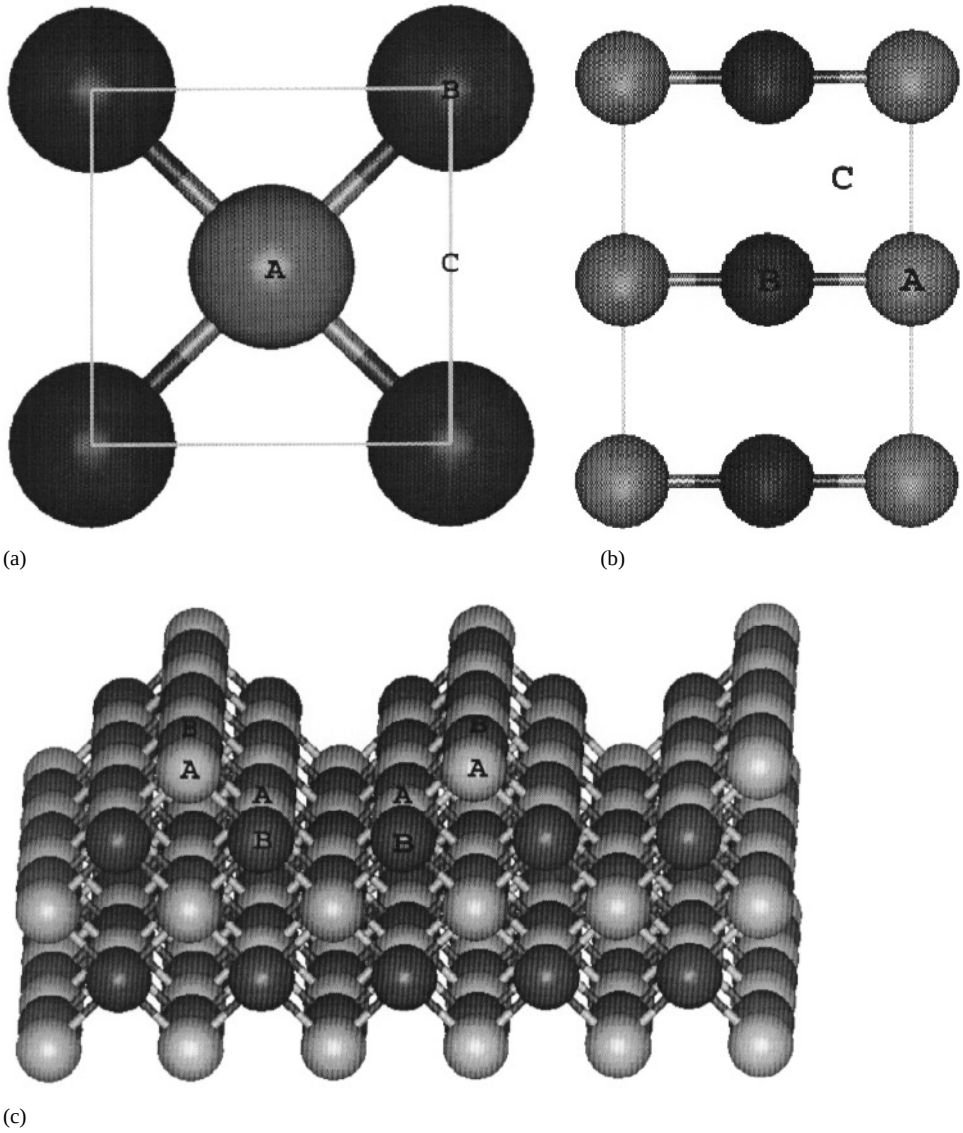


**Figure 1.** (a) MgO{100}, (b) MgO{110}, and (c) MgO{110}$(1 \times 2)$ surfaces. The dark balls represent $Mg^{2+}$ ions and the light balls $O^{2-}$ ions. The silver atoms have been omitted to show the possible location for adsorption. These are A, B and C for the above-$O^{2-}$, above-$Mg^{2+}$, and above-interstitial sites respectively. For the {110}$(1 \times 2)$ interface the most stable configuration is with the Ag atoms above $O^{2-}$ (A) ions. If silver atoms are simultaneously above both a $O^{2-}$ and $Mg^{2+}$ ions (i.e. combinations of A and B) unrealistically short Ag–Ag bonds are formed.

the metal atoms situated above the oxygen ions (table 2). As pointed out by Duffy *et al* [10] in this geometry the distance between the oxide and metal cores is reduced and the image interaction becomes more important and contributed 0.59 J $m^{-2}$ to the work of adhesion. Although it is not possible to compare these results with either *ab initio* calculations or experiment since there are no data yet, the success with the MgO{100}–Ag{100} interface leads us to believe that this model provides a realistic structure and work of adhesion for

**Table 2.** Calculated works of adhesion and wetting angles for MgO–Ag interfaces. The wetting angles were calculated using the Young–Dupre equation and the surface energies for the metal surfaces calculated using the Sutton–Chen potential model ({100} = 0.85 J $m^{-2}$, {110}1 × 1 = 0.92 J $M^{-2}$, and {110}1 × 2 = 0.95 J $m^{-2}$). The term 'unstable' is used to indicate that an energy minimized structure could not be obtained.

| Interaction | Work of adhesion (J $m^{-2}$) | Distance (Å) | Wetting angle ($\phi^{\circ}$) | Image contribution to $W_{ad}$ (J $m^{-2}$) |
|---|---|---|---|---|
| MgO{100}–Ag{100} | | | | |
| Ag over $O^{2-}$ | 0.26 | 2.6 | 133.6 | 0.05 |
| Ag over $Mg^{2+}$ | 0.05 | 3.2 | 164.4 | < 0.01 |
| Ag over interstitial | unstable | | | |
| MgO{110}–Ag{110} planar | | | | |
| Ag over $O^{2-}$ | 1.29 | 1.79 | 66.30 | 1.2 |
| Ag over $Mg^{2+}$ | 0.06 | 2.40 | 159.20 | < 0.01 |
| MgO{110}–Ag{110} reconstructed | | | | |
| Ag over $O^{2-}$ with Ag replacing $Mg^{2+}$ | 0.53 | 2.3–2.7 | 116.2 | 0.01 |
| Ag over $O^{2-}$ with Ag replacing $O^{2-}$ | unstable | | | |
| Ag over $Mg^{2+}$ with Ag replacing $Mg^{2+}$ | −0.44 | 3.0–3.5 | | |
| Ag over $Mg^{2+}$ with Ag replacing $O^{2-}$ | −0.94 | 3.0–4.2 | | |

**Table 3.** MgO{100}–Ag({100} works of adhesion (J $m^{-2}$) for atomistic image plane [10], full-potential linearized muffin tin (FLMTO) [5], linearized augmented plane-wave (FLAPW) [6], and Hartree–Fock (HF) [9] calculations. The experimental result is from [28] and is determined from the observed wetting angle of 135° and using a silver surface energy of 1.53 J $m^{-2}$. The value in parentheses is obtained using the calculated Ag{100} surface energy of 0.85 J $m^{-2}$. We note that in the experimental data [28], although the above oxygen position was favoured, Ag above Mg positions were also observed.

| | Experimental | Image plane | FLMTO | FLAPW | HF |
|---|---|---|---|---|---|
| Ag over O | 0.45(0.25) | 1.05 | 1.52 | 0.64 | 0.36 |
| Ag over Mg | | 1.45 | 0.81 | | 0.11 |
| Ag over hole | | 1.02 | 1.04 | | 0.18 |

this interface.

For both the ideal MgO{100}–Ag{100} and MgO{110}–Ag{110} interfaces we define the metal strain energy as the difference in energy between the free metal slab and the relaxed metal atoms at the interface, and in each case it is less than 0.1 kJ $mol^{-1}$. This indicates that the assumption, made by previous atomistic simulations [10, 11] and *ab initio* calculations [5–9], of holding the metal atoms fixed is valid for these interfaces.

### *3.2. Reconstructed interface*

Recent atomistic simulations [30] have demonstrated that the MgO{110}1 × 1 surface is unstable with respect to the MgO{110}1 × 2 reconstruction whilst the Ag{110}1 × 1 has been shown to be 0.025 J $m^{-2}$ more stable than the missing row {110}1 × 2 surface [22]. Therefore, the reconstructed interface between these surfaces could potentially be the most stable and furthermore emphasizes that this methodology is applicable to an interface of any topology. Faceting of {110} planes in MgO and Ag gives rise to interlocking {100} surfaces (figure 1(c)). Four initial surface geometries were considered: two arise from

the planar interface in which the Ag atoms may lie above either the $O^{2-}$ or $Mg^{2+}$ ions and the two remaining geometries are generated when Ag replaces either an $Mg^{2+}$ of $O^{2-}$ ion at the reconstructed interface. The most stable interface is found to be where the Ag atoms replace the Mg atoms and only Ag–$O^{2-}$ 'bonds' exist (table 2). The remaining configurations contain either only Ag–$Mg^{2+}$ bonds or unreasonable Ag–Ag distances (the substitution of $O^{2-}$ or $Mg^{2+}$ gives rise to an incorrect stacking of the Ag atoms). The work of adhesion of the reconstructed interface is approximately 40% less than that of the non-reconstructed MgO{110}–Ag{110} interface (table 2) and the strain energy is approximately 0.1 kJ $mol^{-1}$. The electrostatic contribution to the work of adhesion is small (approximately 0.01 J $m^{-2}$).

### *3.3. Defective interface*

Stoneham and Tasker [11, 2] proposed that the adhesions across a metal–ceramic interface can be significantly altered by the presence of defects, occurring as either vacancies or impurity ions. Therefore, we considered the effect of vacancies on the work of adhesion.

In the simulations described above the silver atoms prefer energetically to sit above the $O^{2-}$ site. Therefore, defects were introduced into slabs composed of a $2 \times 2$ supercell containing four $O^{2-}$ and four $Mg^{2+}$ ions per layer and the Ag atoms directly above the $O^{2-}$ ions. Although this generates a high density of defects it serves our purpose, which is to demonstrate the effect of defects on metal cohesion to ceramic interfaces. Calculated values for the work of adhesion of several vacancy configurations are given in table 4. Only when an oxygen ion is removed from the top MgO layer is the image attraction across the interface increased to any significant extent (table 4 and figure 2). Indeed, the creation of vacancies in the layers below leads to a slight destabilization of the interface. When the silver atom is placed directly above the vacancy, geometry optimization causes the silver atom to move toward the interface and to reside approximately 0.5 Å above the plane of the remaining oxygen atoms. The strain energy on the metal associated with this configuration is significant (136.5 kJ $mol^{-1}$). Although we calculate the electrostatic potential of a metal atom, charge transfer is not included explicitly and to test this result comparable electronic structure calculations are required to substantiate this. This 'nestling' of metal atoms within the oxide substrate has been postulated before [31] and is thought to induce the so called strong metal support interaction. In figure 2 the work of adhesion is displayed for calculations with and without metal polarization. Polarization of the metal atoms almost triples the work of adhesion when the vacancy is at the surface. The metal polarization also dampens oscillations in energy due to the long-range Coulombic forces (figure 2).

In table 4 we have also presented results where the $Mg^{2+}$ ion is substituted by a dopant cation, X. Where the dopant cation has the same charge as the $Mg^{2+}$ cation (i.e. X = Ca, Sr, Ba) the work of adhesion decreases as the size of ionic radius of the impurity cation increases. Simulations of $Mg^{2+}$ substituted by an $X^{+}$ cation (X = Li, K) and charge compensated by a hole on oxygen suggest that the work of adhesion is dominated by the binding of the hole at the surface.

## 4. Conclusion

We have given details of an efficient method for the calculation of the geometry of metal–ceramic interfaces. The short-range forces between atoms are calculated via analytical functions. The electrostatic interaction across the interface is evaluated by the method

**Table 4.** The work of adhesion (J $m^{-2}$) for various defects at the MgO{100}–Ag{100} interface. The calculations were performed on a $2 \times 2$ supercell with the Ag atoms situated above the O atoms.

| Defect | $W_{ad}$ (J $m^{-2}$) |
|---|---|
| $O^{2-}$ vacancy layer 1 | 6.07 |
| $O^{2-}$ vacancy layer 2 | 0.20 |
| $O^{2-}$ vacancy layer 3 | 0.20 |
| $O^{2-}$ vacancy layer 4 | 0.24 |
| $O^{2-}$ vacancy layer 5 | 0.17 |
| $O^{2-}$ vacancy layer 6 | 0.21 |
| $Ca^{2+}$ substitution for $Mg^{2+}$ | 0.22 |
| $Sr^{2+}$ substitution for $Mg^{2+}$ | 0.17 |
| $Ba^{2+}$ substitution for $Mg^{2+}$ | −0.07 |
| $Li^{+}O^{-}$ substitution for $Mg^{2+}O^{2-}$ (same layer) | 0.28 |
| $Li^{+}O^{-}$ substitution for $Mg^{2+}O^{2-}$ ($Li^{+}$ layer 1, $O^{-}$ layer 2) | 0.18 |
| $Li^{+}O^{-}$ substitution for $Mg^{2+}O^{2-}$ ($O^{-}$ layer 1, $Li^{+}$ layer 2) | 0.30 |
| $K^{+}O^{-}$ substitution for $Mg^{2+}O^{2-}$ (same layer) | 0.25 |

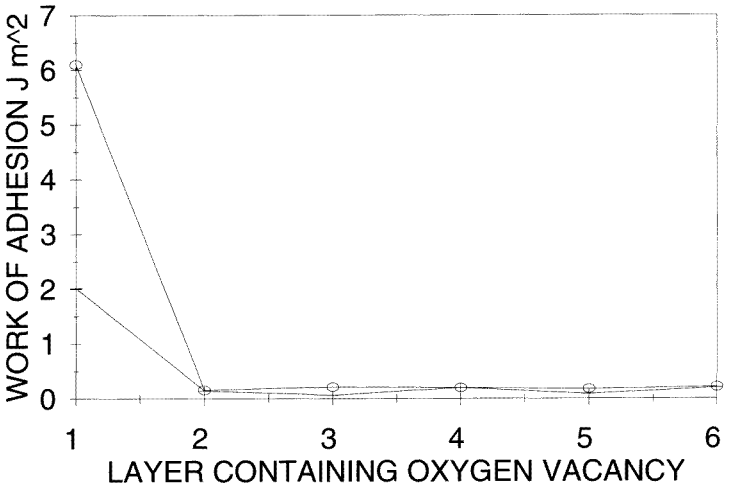


**Figure 2.** Work of adhesion (J $m^{-2}$) as a function of $O^{2-}$ vacancy depth for the MgO{100}–Ag{100} interface. Results are shown with polarization (circles) and without polarization (crosses) of the metal atoms.

described by Finnis *et al* [15], which can easily be incorporated into an Ewald type summation. Using this computational technique we have examined the structure and work of adhesion of both ideal and irregular interfaces.

The evaluation of this model is difficult since there have been few experiments describing the atomic arrangement and we have to rely, in part, on a comparison with previous electronic structure calculations. However our calculated wetting angle for the MgO{100}–Ag{100} interface is in good agreement with experiment. We also find that the silver atoms prefer to lie above the oxygen ions, which is in agreement with electronic structure calculations, particularly the FLAPW [6] and Hartree–Fock [9] results. We have demonstrated that charged defects and impurities will play an important role in metal–

ceramic adhesion; however further comparison with electronic structure calculations would be useful. The metal atoms adjust their positions to accommodate the defects and the strain energy associated with this can be large. Our methodology could be used in conjunction with detailed electronic structure calculations to identify good candidates for study and to obtain reliable starting configurations.

With the success of the above calculations we hope to apply this technique to technologically important interfaces (e.g. Rh–$TiO_2$, growth of oxide scales on Ni–Fe) and to study the effect of temperature on metal–ceramic adhesion via molecular dynamics.

## Acknowledgments

We would like to thank Drs J H Harding and M W Finnis for helpful discussions, the EPSRC for financial support, and Biosym technologies for Insight II.

## References

[1] Howe J M 1993 *Int. Mater. Rev.* **38** 233
[2] Klomp J T 1989 *Surfaces and Interfaces of Ceramic Materials* ed L C Dufour (Norwell, MA: Kluwer) p 375
[3] Nichols M G 1988 *Mater. Sci. Forum.* **29** 127
[4] Adamson A W 1960 *Physical Chemistry of Surfaces* (New York: Interscience)
[5] Schonberger U, Anderson O K and Methfessel M 1992 *Acta. Metall. Mater.* **40** S1
[6] Li C, Wu R, Freeman A J and Fu C L 1993 *Phys. Rev.* B **48** 8317
[7] Kruse C, Finnis M W, Milman V Y, Payne M C, DeVita A and Gillan M J 1994 *J. Am. Ceram. Soc.* **77** 431
[8] Smith J R, Hong T and Srolovitz D J 1994 *Phys. Rev. Lett.* **72** 4021
[9] Heifets E, Kotomin E A and Orlando R 1996 *J. Phys.: Condens. Matter* **8** 6577
[10] Duffy D M, Harding J H and Stoneham A M 1992 *Acta. Metall.* **40** 511
[11] Duffy D M, Harding J H and Stoneham A M 1993 *Phil. Mag.* **67** 865
[12] Stoneham A M and Tasker P W 1985 *J. Phys. C: Solid State Phys.* **18** L543
[13] Stoneham A M and Tasker P W 1987 *Ceramic Microstructures*, ed J A Pask (New York: Plenum) p 155
[14] Duffy D M, Harding J H and Stoneham A M 1995 *Acta. Metall. Mater.* **43** 1559
[15] Finnis M W, Stoneham A M and Tasker P W 1990 *Metal–Ceramic Interfaces*, ed M Ruhle *et al* (Oxford: Pergamon) p 35
[16] Parry D E 1976 *Surf. Sci.* **54** 195
[17] Sangster M J L and Stoneham A M 1981 *Phil. Mag.* B **43** 597
[18] Finnis M W and Sinclair J E 1984 *Phil. Mag.* A **50** 45
[19] Ackland G J, Tichy G, Vitek V and Finnis M W 1987 *Phil. Mag.* A **56** 735
[20] Sutton A P and Chen J 1990 *Phil. Mag. Lett.* **61** 139
[21] Hammonds K D and Lynden-Bell R M 1992 *Surf. Sci.* **278** 437
[22] Todd B D and Lynden-Bell R M 1993 *Surf. Sci.* **281** 191
[23] Finnis M W, Kaschner R, Kruse C, Furthmuller J and Scheffler M 1995 *J. Phys.: Condens. Matter* **7** 2001
Finnis M W 1991 *Surf. Sci.* **241** 61
[24] Gordon R G and Kim Y S 1972 *J. Chem. Phys.* **56** 3122
[25] Allan N L and Mackrodt W C 1994 *Phil. Mag.* B **69** 871
[26] Slater J C and Kirkwood J G 1931 *Phys. Rev.* **37** 682
[27] Wood C P and Pyper N C 1986 *Phil. Trans. R. Soc.* A **320** 71
[28] Trampert A, Ernst F, Flynn C P, Fischmeister H F and Ruhle M 1992 *Acta. Metall. Mater.* **40** s227
[29] Guénard P, Renaud G and Villette B 1996 *Physica* B **221** 205
[30] de Leeuw N H, Watson G W and Parker S C *J. Phys. Chem.* at press
[31] Sanchez M G and Gazquez J L 1987 *J. Catal.* **104** 120